Biomicrofluidics ARTICLE scitation.org/journal/bmf

3D collagen microchamber arrays for combined chemotherapy effect evaluation on cancer cell numbers and migration

Cite as: Biomicrofluidics **17**, 014101 (2023); doi: 10.1063/5.0121952
Submitted: 21 August 2022 · Accepted: 5 December 2022 ·
Published Online: 3 January 2023

Jingru Yao,[1] Guoqiang Li,[2,a)] Lianjie Zhou,[1] Shuyan Xu,[1] Kena Song,[3] Hongfei Zhang,[4] Xianquan Zhang,[4] Jianwei Shuai,[5,6] Fangfu Ye,[6,7] Ming Li,[5] Guo Chen,[1] He Liu,[8] Peter Shaw,[8,a)] and Liyu Liu[1,a)]

AFFILIATIONS

[1]Chongqing Key Laboratory of Soft Condensed Matter Physics and Smart Materials, College of Physics, Chongqing University, Chongqing 401331, China
[2]Chongqing Key Laboratory of Environmental Materials and Remediation Technologies, College of Chemistry and Environmental Engineering (Chongqing University of Arts and Sciences), Chongqing 402160, People's Republic of China
[3]College of Medical Technology and Engineering, Henan University of Science and Technology, Henan 471023, China
[4]Hygeia International Cancer Hospital, Chongqing 401331, China
[5]Beijing National Laboratory for Condensed Matter Physics, Institute of Physics, Chinese Academy of Sciences, Beijing 100190, China
[6]Department of Physics, Xiamen University, Xiamen 361005, China
[7]Wenzhou Institute, University of Chinese Academy of Sciences, Wenzhou 325000, China
[8]Oujiang Laboratory (Zhejiang Lab for Regenerative Medicine, Vision and Brain Health), Wenzhou, Zhejiang 325000, China

[a)]**Author to whom correspondence should be addressed:** guoqiangli1989@126.com; petershaw@ojlab.ac.cn; and lyliu@cqu.edu.cn

ABSTRACT

Breast cancer metastasis involves complex mechanisms, particularly when patients are undergoing chemotherapy. In tissues, tumor cells encounter cell–cell interactions, cell–microenvironment interactions, complex nutrient, and drug gradients. Currently, two-dimensional cell culture systems and animal models are challenging to observe and analyze cell responses to microenvironments with various physical and bio-chemical conditions, and microfluidic technology has been systematically developed to address this dilemma. In this study, we have constructed a combined chemotherapy evaluation chip (CCEC) based on microfluidic technology. The chip possesses 192 diamond-shaped microchambers containing MDA-MB-231-RFP cells, and each microchamber is composed of collagen to mimic breast cancer and its surrounding microenvironment. In addition, by adding medium containing different drugs to the medium channels of CCEC, composite drug (paclitaxel+gemcitabine+7rh and paclitaxel+fluorouracil+PP2) concentration gradients, and single drug (paclitaxel, gemcitabine, 7rh, fluorouracil, PP2) concentration gradients have been established in the five collagen regions, respectively, so that each localized microchamber in the regions has a unique drug microenvironment. In this way, we evaluated the composite and single chemotherapy efficacy on the same chip by statistically analyzing their effects on the numbers and migration of the cell. The quantitative results in CCECs reveal that the inhibition effects on the numbers and migration of MDA-MB-231-RFP cell under the composite drug gradients are more optimal than those of the single drugs. Besides, the cancer cell inhibition effect between the groups composed of two drugs has also been compared, that is the paclitaxel+gemcitabine, paclitaxel+fluorouracil, and paclitaxel+PP2 have better cell numbers and migration inhibition effects than paclitaxel +7rh. The results indicate that the bio-mimetic and high-throughput combined chemotherapy evaluation platform can serve as a more efficient and accurate tool for preclinical drug development and screening.

I. INTRODUCTION

Breast cancer seriously threatens women's health.[1] Although the treatment of primary breast tumors has been significantly improved, the systematic treatment of metastatic breast cancer is less effective. Metastasis is the root cause of death for most patients with breast cancer.[2] In the past decades, many studies have shown that the invasion and metastasis of breast cancer are closely related to the microenvironment in which the cancer cells are located.[3] Therefore, fabricating *in vitro* cultured model systems that can simulate the microenvironment *in vivo* is crucial in cancer research.[4]

However, it is still a significant deficiency that the most common research models in life science are two-dimensional (2D) cell cultures and animal models. Among them, 2D cell culture environments differ immensely from the three-dimensional (3D) microenvironment in the human body, resulting in changes in cell morphological and physiological characteristics, which may lead to a contradictory interpretation of the experiments.[5,6] In contrast, although animal experimental results are usually more reliable than common cell culture, they also have the weakness of being expensive and time-consuming.[7] To address this drawback, many new developments that construct 3D culture models *in vitro* in microfluidic technology have been made.[8] It can simulate tumor structures *in vivo* and study the cell–cell and cell–microenvironment interaction. Notably, the use of microfluidic chips to build *in vitro* "battlefields" for cancer cell growth, invasion, and metastasis has significantly improved breast cancer research and diagnosis.[9–11] For example, some researchers have successfully developed lab-on-a-chip (LOC) or organ-on-a-chip (OOC) to investigate cancer cell invasion and metastasis mechanisms of cancer cells in complex tissue environments.[12] These models accurately control the local microenvironment, simulate the function of human organs, and avoid expensive animal tests, so they are considered as *in vitro* platforms for cancer research that could replace the 2D cell culture and animal models.[13]

Besides fundamental research, microfluidic chip-based *in vitro* cancer models also have great potential to provide meaningful preclinical drug screening.[14] Current cancer treatments include chemotherapy, surgery, and radiation therapy. Among these, drug chemotherapy is one of the important means of breast cancer treatment.[15] Figure 1(a) shows a breast cancer patient with combined chemotherapy and the heterogeneous *in vivo* tumor microenvironment. The left is a diagram of a patient with breast cancer who is given multiple anti-cancer drugs, with the mammary gland (pink) and breast cancer (red). To its immediate right is a zoom-in on the breast tumor and its surrounding heterogeneous microenvironment, which contains breast cancer cells (red) and the extracellular matrix (ECM) composed of collagen (gray), as well as drug I (red), drug II (blue), and drug III (green). To achieve better treatment effects for cancer patients, anti-cancer drugs' combination chemotherapy has been generally accepted as a feasible strategy in clinical practice, which can reduce drug resistance and side effects.[16,17] Currently, the standard method to evaluate the efficacy of combination chemotherapy regimens is to use clinical trials, which are systematic studies of human drugs.[18,19] However, clinical trials require a large amount of workforce and time, are expensive, and often impose a tremendous burden on patients.[20,21]

Given the current challenges in the evaluation of combination chemotherapy, our study developed the combined chemotherapy evaluation chip (CCEC) based on the tumor microenvironment in breast cancer patients that receive combination chemotherapy. As shown in Fig. 1(b), the drugs simultaneously form a stable composite concentration gradient and multiple single concentration gradients through its diffusion in the collagen microenvironment on the same chip. In that case, cancer cells of the same batch at different locations in each region will be in a local microenvironment with varying concentrations of the drugs. By combining this platform with microscopy imaging and immunofluorescence technology, we conducted the high-throughput statistical and comparative analysis of the efficacy of using composite drugs, single drug, and drug-free, and further efficiently evaluate the effect of combination chemotherapy on cancer cells. The CCEC system can be used for preliminary evaluation of the efficacy of combination chemotherapy before clinical trials, improve the success rate of clinical trials, and save a lot of manpower and materials. CCEC system has critical clinical value for providing drug guidance programs for patients in the short term in the future.

II. MATERIALS AND METHODS

A. Cell culture

The breast cancer cell line MDA-MB-231-RFP in CECC was obtained from China Infrastructure of Cell Line Resources (Beijing, China). MDA-MB-231-RFP cells were cultured in RPMI (Corning, NY, USA) supplemented with 10.0% (v/v) fetal bovine serum (Gibco, NY, USA) and 1.0% (v/v) penicillin/streptomycin (Corning, NY, USA), and placed in a 37.0 °C incubator containing 5.0% CO_2. During the experiment, the cell density of MDA-MB-231-RFP cells seeded into CCEC was 3.0×10^6 cells/ml.

B. Collagen preparation

Collagen is a bio-compatible material often used to construct extracellular matrices *in vitro*. It is a porous structure that provides physical support for cells and is an essential medium during the transport and diffusion of biochemical substances.[22] Therefore, in CCEC systems, we selected collagen I extracted from rat tail (354236, Corning, NY, USA) to construct the extracellular microenvironment and study the numbers and migration of cell in the microenvironment.[23] Collagen (the concentration of 10.27 mg/ml) was diluted with 10×PBS (Corning, NY, USA) and sterile water to 5.0 mg/ml, pH level was adjusted to 7.2. The average pore area and pore size of solidified collagen were 82.66 μm^2 and 5.13 μm, respectively, as calculated by the SEM image (Fig. S1 in the supplementary material). Studies show that the matrix conditions with different collagen concentrations significantly impact the growth and migration of cancer cells and the drug efficacy for limiting cell migration, the range of collagen concentrations commonly used to construct cancer cell migration models is 1.0–6.0 mg/ml.[24–26] In our study, after many tests, 5.0 mg/ml collagen is more suitable for constructing the extracellular matrix in CCEC, which can maintain the sound diffusion of drug molecules and has excellent stability to meet the long-term tracking experiment of 120.0h. In contrast, other collagen concentrations are currently not suitable for this system.

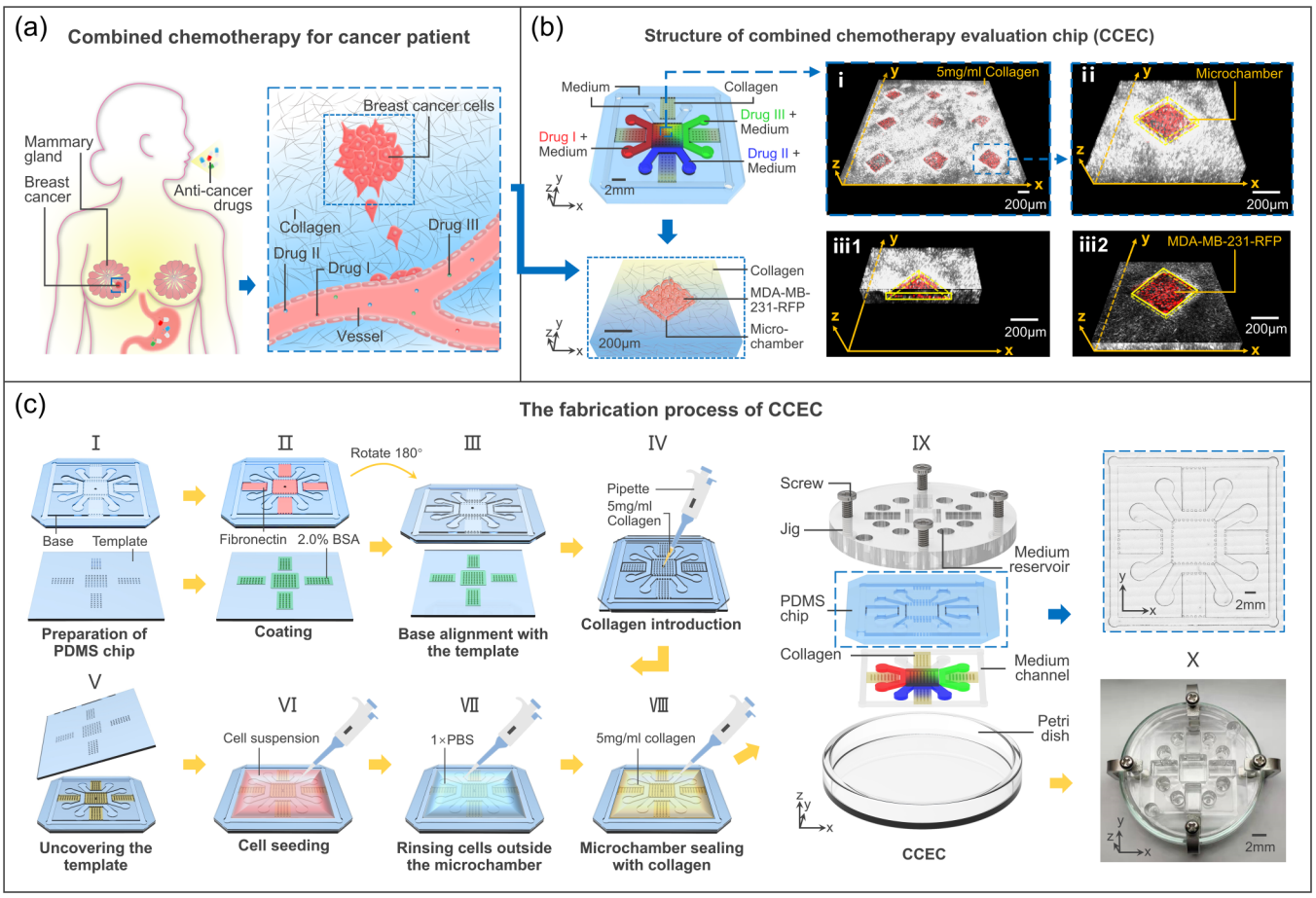

FIG. 1. The design of CCEC is based on the biochemical microenvironment in breast cancer patients. (a) Schematic illustration of the biochemical microenvironment in breast cancer patients treated by combination chemotherapy. (b) The design of CCEC and its microchamber. The upper left shows a schematic view of CCEC, which mainly includes medium channels and collagen regions. The lower left illustrates the schematic enlarged view of a single microchamber in the chip. Right (i) shows an image of nine microchambers captured by a confocal microscope (SP8, Leica, Germany), (ii) is a magnified view of one of the microchambers, and (iii1–iii2) are 3D cross sections of a single microchamber in the x-z plane, and x-y plane, respectively. The microchamber (yellow) is composed of collagen (white), and MDA-MB-231-RFP cells (red). (c) The fabrication process of CCEC.

C. The design of CCEC

Following the diagram shown in Fig. 1(a), CCEC was designed and illustrated on the upper left side of Fig. 1(b). The chip mainly contains five medium channels and five drug evaluation regions. During the experiment, the five channels were injected with medium (peripheral channel and upper channel), medium containing drug I (left channel, red), drug II (lower channel, blue), and drug III (right channel, green). These five channels divide the chip into five drug evaluation regions: composite drug evaluation region (middle), single drug evaluation region (left, lower and right), and no drug evaluation region (upper). In every drug evaluation region, each diamond-shaped closed microchamber was surrounded by collagen, which contained breast cancer MDA-MB-231-RFP cells, as shown in the lower left side of Fig. 1(b). Our previous research shows that cancer cells in the circular microchamber cannot break through the annular collagen fiber microenvironment to migrate in a short period.[27] Thus, the microchamber is unsuitable to be designed as a circle shape, while the diamond microchamber composed of collagen fiber is more advantageous to cancer cell migration and suitable for studying the effect of different drug microenvironment of cancer cells. In CCEC, the composite drug evaluation region contains 64 microchambers, and the single drug evaluation regions and no drug evaluation region contain 32 microchambers. In that case, each microchamber in the drug evaluation region is in a unique biochemical microenvironment, the tumors *in vivo* in different drugs.

D. The fabrication process of CCEC

The fabrication process of CCEC is shown in Fig. 1(c). Initially, the PDMS chip was prepared using soft etching

technology, including base (blue) and microchamber template (blue) (step I). Then, the base was incubated with fibronectin (Corning, NY, USA) (pink) at 37.0 °C for 2.0h, which allowed collagen to cling firmly to the base. Concurrently, the microchamber template was incubated with 2.0% bovine serum albumin (BSA, Cell Signaling Technology, USA) (green) at room temperature for 2.0h to detach the collagen from the template (step II). After that, the base was turned over 180°, aligned with the microchamber template, and attached, and thus a cavity was formed between the two (step III). Subsequently, 5.0 mg/ml collagen was injected into the cavity through the gel injection hole in the center of the base (step IV). After the collagen was solidified, the chip was turned over again; the microchamber template was uncovered and discarded. At this point, a diamond-shaped microchamber composed of collagen was formed on the base (step V). Next, the cell suspension was spread on the base (step VI); after the cancer cells fell into the microchamber, the cancer cells outside the microchamber were rinsed off with 1×PBS (step VII). Then, the microchambers containing cancer cells were sealed with 5.0 mg/ml collagen (step VIII). Finally, CCEC was fixed with a jig containing a culture pool and a Petri dish seated in a live cell culture apparatus (Okolab, Italy) for 120.0h. During the experiment, the medium was renewed every 24.0h, and the chip was imaged simultaneously. The top right is a microscope image of the base (step IX), and the bottom right is the physical image of CCEC (step X).

E. Immunofluorescence analysis

The immunofluorescence of specific proteins can be used to test the effectiveness of drugs in the CCEC system. After the drug evaluation was completed, the jig and Petri dish on the CCEC were removed, and the medium was washed off with pre-warmed (37.0 °C) 1 × PBS (Corning, NY, USA). Subsequently, the pre-warmed (37.0 °C) 4.0% paraformaldehyde (Beyotime, MA, USA) was spread over the chip for 1.0h, and the MDA-MB-231-RFP cells in the chip were fixed. Next, the 4.0% paraformaldehyde was cleaned with 1×PBS. The chip was infiltrated with normal goat serum (Solarbio, China) and seated at 37.0 °C in the dark for 3.0h. The normal goat serum was then removed. After that, the DDR1 primary antibody reagent DDR1 (D1G6) XP Rabbit mAb (Cell Signaling Technology, MA, USA) was diluted with 1 × PBS at a ratio of 1:200, spread over the chip, and kept in a 4.0 °C incubator for 12.0h. Then, the primary antibody was washed off with 1 × PBS to complete the labeling of the DDR1 protein. The secondary antibody reagent Streptavidin-Alexa Fluor 555 antibody (Bioss, China) combined with the primary antibody, labeled the DDR1 protein as yellow fluorescence, and was diluted with 1 × PBS at a ratio of 1:300. The diluted secondary antibody solution was spread over the chip and was allowed to stand at 37.0 °C for 2.0h. Finally, the secondary antibody was washed off with 1 × PBS. Afterward, images were taken with the yellow fluorescence channel of a confocal microscope (SP8, Leica, Germany). The primary and secondary antibodies used for E-cad protein staining were E-Cadherin (24E10) Rabbit mAb (Cell Signaling Technology, MA, USA) and Streptavidin-Alexa Fluor 350 antibody (Bioss, China), respectively. The operation procedure was the same as above, and the images were taken with the blue fluorescence channel of the confocal microscope.

III. RESULTS AND DISCUSSION

A. Simulation and construction of concentration gradients in the chip

One of the advantages of CCEC is that it contains five collagen gel regions formed by the trapezoidal micropillar array barrier and five independent medium channels around the gel regions [shown in Fig. 1(b)]. The channels are filled with medium containing different drugs, diffusing through the gaps in the micropillar array into the gel region. Thus, different drug concentration gradients could simultaneously form in each gel region. To examine the space-time relationship of drug concentration gradient formation, we selected Rhodamine-dextran (4 kDa, red), Cascade Blue-dextran (3 kDa, blue), and FITC-dextran (4 kDa, green) with the same type as drug molecules, they are both organic and water-soluble molecules and diffuse in the form of molecules in collagen gel. These dye molecules have been widely used in drug gradient tests.[27–29] First, COMSOL (Multiphysics 5.6, Comsol, Sweden) software was used to simulate the diffusion of the three dyes in CCEC, confirming that a stable gradient was formed in the gel region of the chip. During the simulation, we used the "Transport of Diluted Species" physics field in the COMSOL software to simulate the diffusion of dyes in collagen. The initial concentration of the dyes and the porosity of collagen gel were set as 10.0 μg/ml and 36.8%. As shown in Fig. 2(a), the three dyes diffused to the adjacent gel regions, forming a composite concentration gradient and three single concentration gradients. Apparently, the closer the channels, the higher the dye concentration [shown in Figs. 2(a) and 2(b)]. Hence, the results indicate that our designed CCEC should be able to form stable single and composite biochemical concentration gradients through the diffusion of biochemical factors or small molecular compounds in collagen gels.

Next, to verify the COMSOL simulation results, CCEC was constructed according to the fabrication process shown in Fig. 1(c). During the experiment, the experimental parameters were consistent with the simulation parameters. The three-dye solutions were added to the prepared CCEC, refreshed every 24.0h, and imaged by an inverted fluorescence microscope (Ti-E, Nikon, Japan) to visualize the concentration gradients in the gel region. As shown in Fig. 2(c), when the dye solution entered the channel, it gradually diffused to the adjacent gel regions, forming three single dye concentration gradients (I–III) and a composite dye concentration gradient (IV) in the chip. The fluorescence intensities of the three dyes over time and space were computed using a MATLAB script. It shows that the fluorescence intensity of each dye at a specific position is inversely proportional to the distance from the position to the dye channel, and the dye gradients in each region remain almost unchanged at 24, 48, 72, 96, and 120h, indicating that a continuous and stable concentration gradient can be formed in collagen region after 24h of dye diffusion. The result, that collagen with porous structures can maintain a stable biochemical concentration gradient, is consistent with previous research as Ref. 30. Therefore, the CCEC system can combine optical imaging

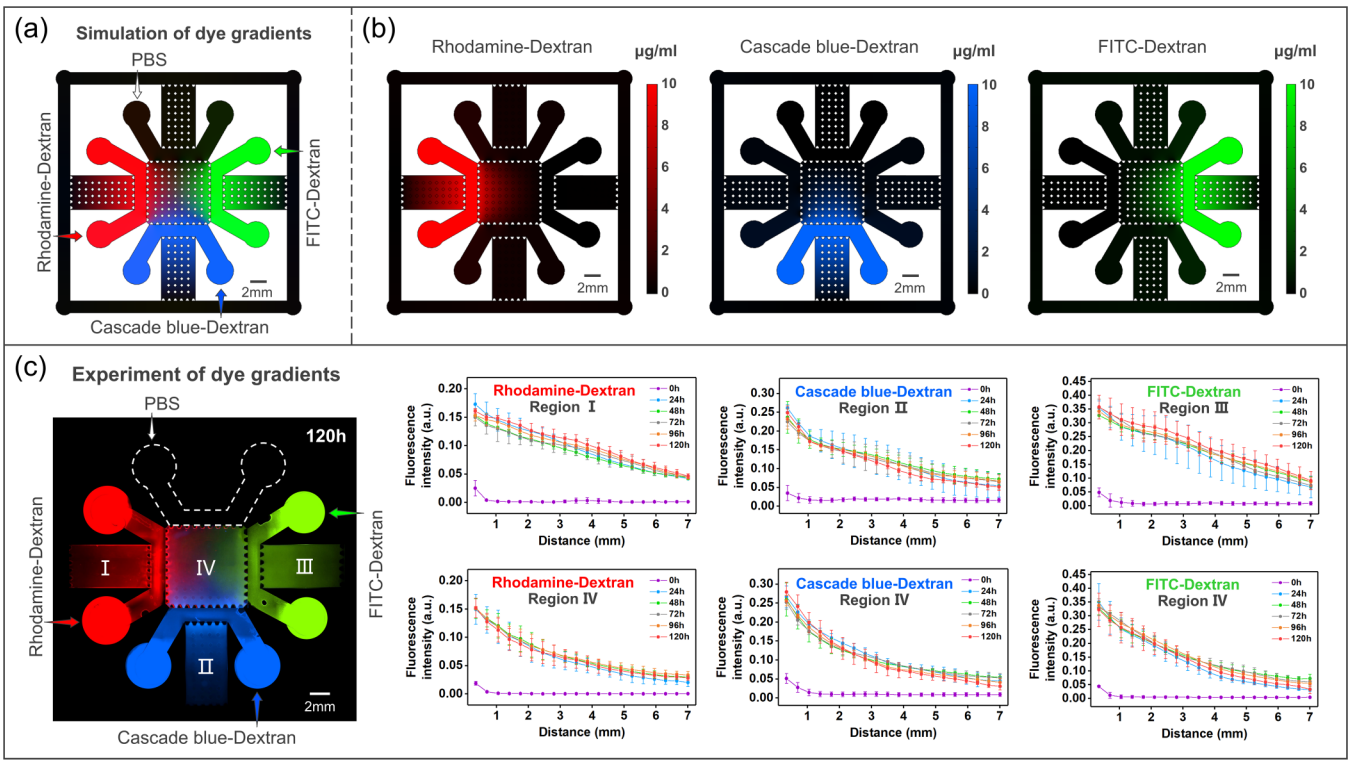

FIG. 2. Simulation and construction of dye gradients. (a) and (b) COMSOL simulation of Rhodamine-Dextran (red), Cascade Blue-Dextran (blue), and FITC-Dextran (green) diffusion in the CCEC. (c) The left inset shows the stable dye gradients of 120.0h constructed in CCEC. The six statistical graphs on the right show the fluorescence intensity distribution of Rhodamine-Dextran, Cascade Blue-Dextran, and FITC-Dextran at different locations in different regions and at different times (0, 24.0, 48.0, 72.0, 96.0, and 120.0 h). The X axis represents the distance between a location in a region of the chip and a dye channel, such as the distance between a location in region I and the Rhodamine-Dextran channel. The Y axis represents the fluorescence intensity of the dye.

technology to provide an excellent experimental platform for high-throughput drug combination screening.

B. Spatial dynamics of breast cancer cell numbers and migration in anti-cancer drug gradients

Another advantage of CCEC is that the chip contains 192 enclosed microchambers composed of collagen, each of which can serve as an independent research unit, providing cancer cells in the microchamber with a 3D culture microenvironment like that *in vivo*. By adding the medium containing different drugs to the microfluidic channels of the chip, stable drug concentration gradients are formed in various regions of the chip. In that case, each microchamber in each region is in a different local biochemical microenvironment. Therefore, combined with optical imaging and quantitative analysis, it is promising to assess the effect of single and composite drug gradients on cells in the microchamber at high-throughput levels.

To test this function of the chip, we selected several breast cancer chemotherapy drugs. First, the three anti-cancer drugs were injected on opposing sides of a central region so that the concentration of these drugs spread across the central region in the CCEC system. Doing so allowed the inhibition effect of the various composite drugs on the numbers and migration of breast cancer cell to be observed. There were also three regions in our chip design containing only one drug. A control region that contained no drugs was also placed on the chip [Figs. 3(a) and 4(a)].

Among the drugs considered, paclitaxel (PTX) is a commonly used first-line drug.[31,32] Gemcitabine (GEM) is an anti-cancer drug widely used in the clinical treatment of breast cancer.[33] Paclitaxel combined with gemcitabine has been used clinically.[34] 7rh is a discoidin domain receptor 1 (DDR1) inhibitor that reduces the interaction between cancer cells and collagen by inhibiting the expression of DDR1 and thus inhibits the migration of cancer cells, 7rh is not currently in use in clinical practice.[35,36] Previous studies demonstrated that long-term use of a single drug leads to resistance to the drug, resulting in unsatisfactory efficacy, while synergistic combination drugs can reduce drug resistance and improve drug efficacy.[37–39] Therefore, we tested the effects of single and composite drugs on cells under the anti-cancer drug group PTX+GEM+7rh in the CCEC system [shown in Fig. 3(a)]. Figure 3(b) shows the enlarged image of MDA-MB-231-RFP cells (red) and MDA-MB-231-RFP cells off-chamber migration under the anti-cancer drug group PTX+GEM +7rh for 120.0h. Specifically, under the single drug gradients (a_1–c_1),

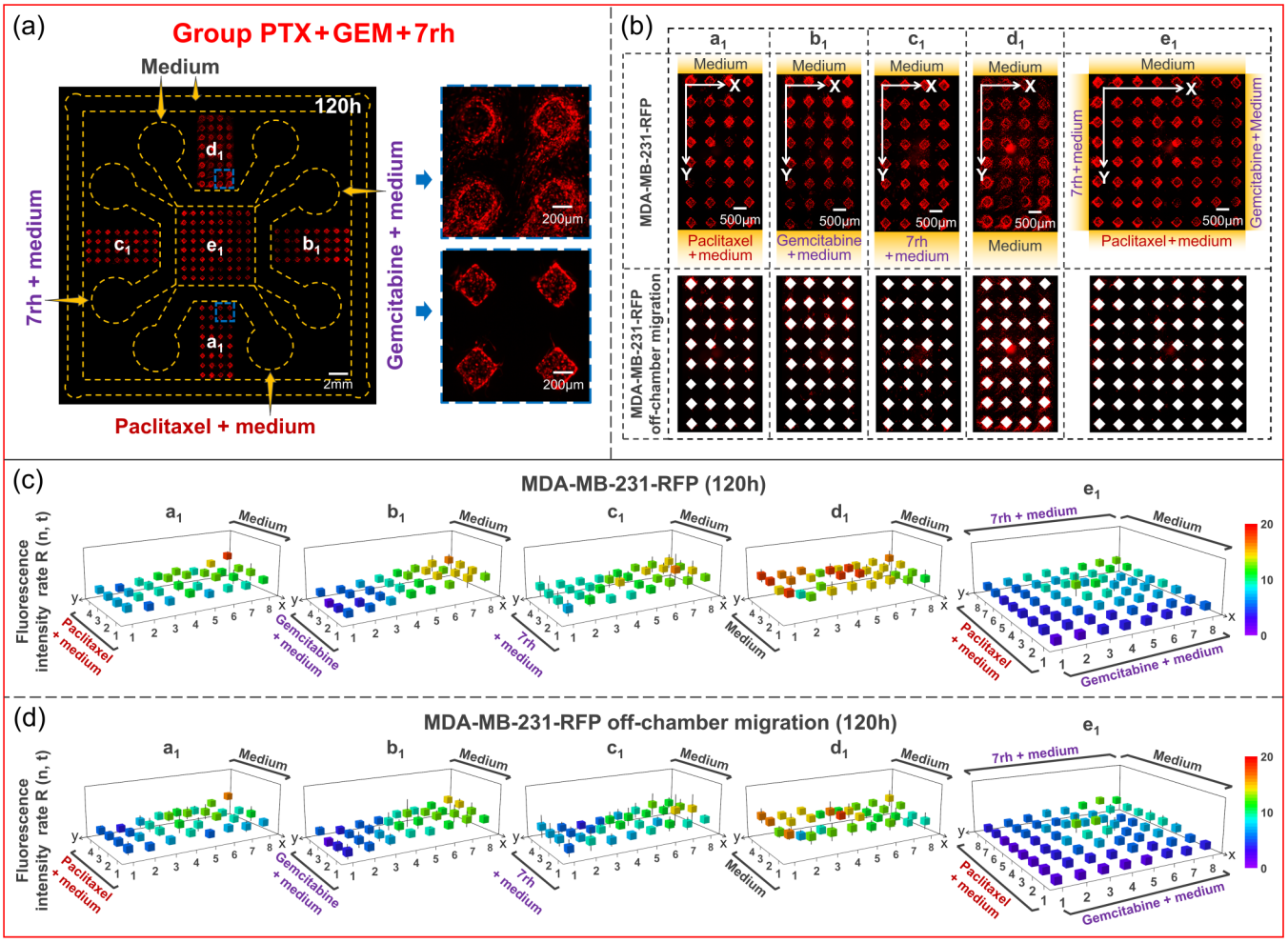

FIG. 3. The evaluation of the effects of the anti-cancer drug group PTX+GEM+7rh on the numbers and migration of cancer cells. (a) MDA-MB-231-RFP cell (red) distribution at 120.0 h in drug gradients. Inside the blue dotted line is an enlarged view of the microchambers in the chip. During the experiment, paclitaxel (31.00 ng/ml), 7rh (44.88 μg/ml), gemcitabine (19.00 ng/ml), and medium were introduced into the channels. (b) The chip is divided into five regions and marked as (a_1)–(e_1). The fluorescence images in the first row represent the numbers of MDA-MB-231-RFP cell, while the images in the second row represent the migration of MDA-MB-231-RFP cells out of the microchamber, and the white represents the removal of the microchamber. (c) and (d) The fluorescence intensity rates of MDA-MB-231-RFP cells and MDA-MB-231-RFP cells off-chamber migration in each region at 120.0 h. Purple to red indicates the fluorescence intensity rates from low to high.

MDA-MB-231-RFP cell numbers and migration were changed along the direction of the diffusion of the drugs, but there was no significant difference in the drug-free region (d_1). Under the composite drug gradient (e_1), we find significant differences in different local regions. Such as, the local regions with higher concentrations of paclitaxel and gemcitabine have more substantial inhibitory effects on cells. This distribution indicates that the CCEC system can be used for high-throughput initial evaluation of single and composite drug effects through cell numbers and migration.

Subsequently, to quantitatively analyze the numbers and migration of MDA-MB-231-RFP cell over time under the drug concentration gradient in each region. According to the studies, the fluorescence intensity of RFP-labeled cells is a reasonable parameter to indicate the numbers of cells.[40] Therefore, we evaluated the effect of the drug concentration gradients by dividing and analyzing the fluorescence images of MDA-MB-231-RFP cells at any time point relative to 0h. Specifically, each of the three single drug regions and one drug-free region was divided into 32 sub-regions, and the composite drug region was divided into 64 sub-regions. Then, the fluorescence intensity of each sub-region was analyzed by MATLAB. The fluorescence intensity of cells in a specific sub-region n and time t defines as I (n, t), where $n = 0, 1, \ldots, 32$ or $n = 0, 1, \ldots, 64$, and $t = 0, 24, \ldots, 120$h. To analyze cell behavior within each sub-region, the cell fluorescence intensity rate R (n, t) defines as

$$R(n, t) = I(n, t)/I(n, 0), \quad (1)$$

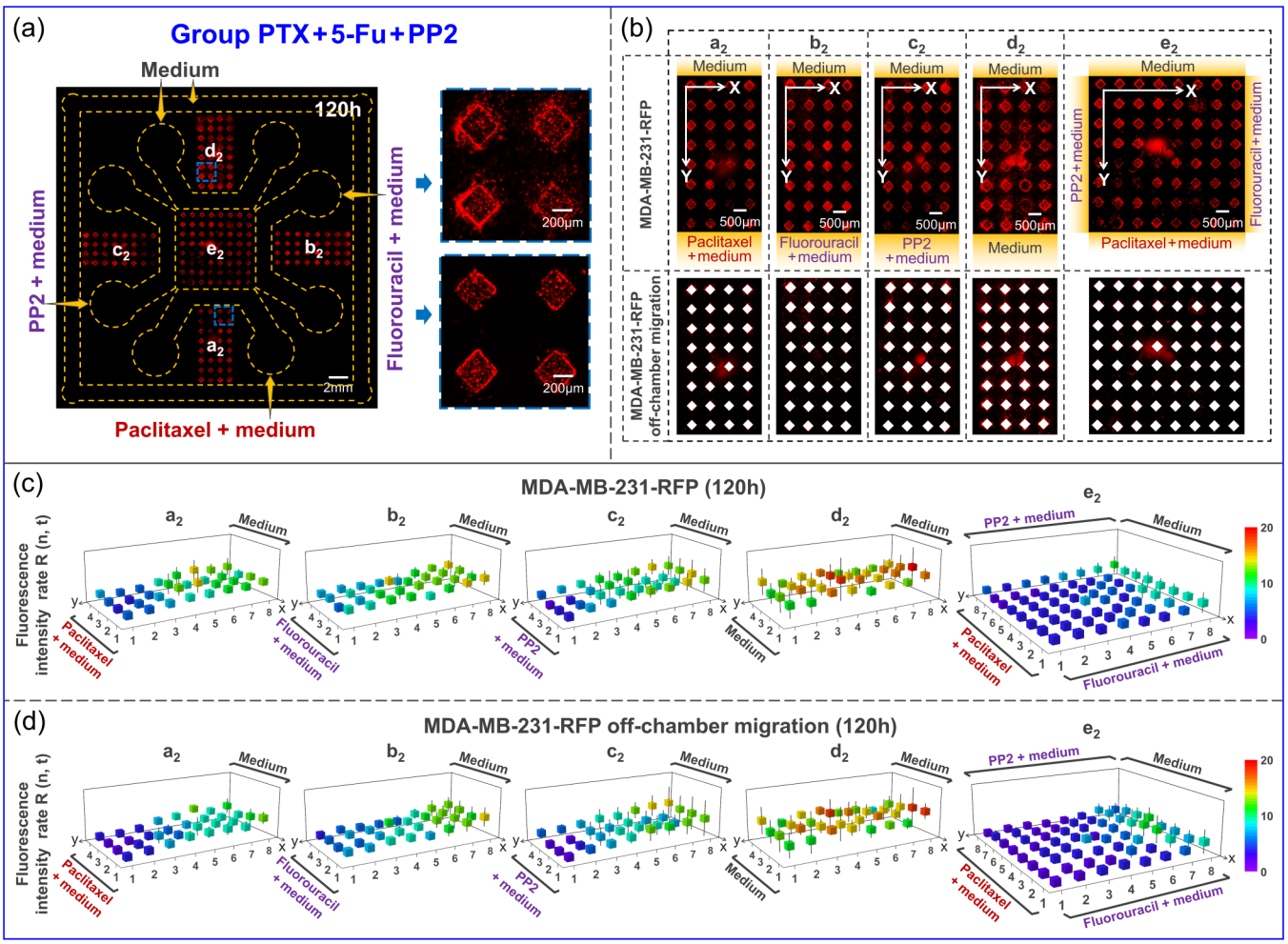

FIG. 4. The evaluation of the effects of the anti-cancer drug group PTX+5-Fu+PP2 on the numbers and migration of cancer cell. (a) MDA-MB-231-RFP cells (red) distribution at 120.0 h in drug gradients. Inside the blue dotted line is an enlarged view of the microchambers in the chip. During the experiment, paclitaxel (31.00 ng/ml), PP2 (150.87 μg/ml), fluorouracil (2.50 μg/ml), and medium were introduced into the channels. (b) The chip is divided into five regions and marked as (a_2)–(e_2). The fluorescence images in the first row represent the numbers of MDA-MB-231-RFP cell, while the images in the second row represent the migration of MDA-MB-231-RFP cells out of the microchamber, and the white represents the removal of the microchamber. (c) and (d) The fluorescence intensity rates of MDA-MB-231-RFP cells and MDA-MB-231-RFP cells off-chamber migration in each region at 120.0 h. Purple to red indicates the fluorescence intensity rates from low to high.

where I (n, 0) is the fluorescence intensity of cells in sub-region n at 0h, and I (n, t) is the fluorescence intensity of cells in sub-region n at t h. In this study, the fluorescence intensity rate of MDA-MB-231-RFP cells and MDA-MB-231-RFP cells off-chamber represent cell numbers and migration, respectively, as shown in Fig. S2 and S3 in the supplementary material. Moreover, the drugs had little effect on cells within 72.0h, and the analysis of the fluorescence intensity rate within this time may not provide more valuable information, so we mainly analyzed the fluorescence intensity rate of the cells at 120.0h.

Figures 3(c) and 3(d) show the spatial distribution diagram of the fluorescence intensity rate of MDA-MB-231-RFP cell numbers and migration at 120.0h, respectively. Under the single drug gradient of paclitaxel (a_1), gemcitabine (b_1), and 7rh (c_1), the fluorescence intensity rate of cells is low and changes from low to high from the side containing drugs to the side without drugs. In contrast, the fluorescence intensity rate of cells in the drug-free region (d_1) is higher and exhibits non-spatial differences. These results illustrate that paclitaxel, gemcitabine, and 7rh have formed stable drug gradients in their respective regions and affected the numbers and migration behavior of MDA-MB-231-RFP cell. Moreover, under the composite gradient of the three drugs (e_1), the fluorescence intensity rate of cells in the local area with higher concentrations of paclitaxel combined with gemcitabine (paclitaxel +gemcitabine, bottom left), as well as paclitaxel combined with 7rh (paclitaxel+7rh, upper left), are lower than those of

gemcitabine and 7rh single drug gradients, respectively. Meanwhile, the local fluorescence intensity rate of paclitaxel +gemcitabine is lower than that of paclitaxel+7rh. Therefore, these results show that the concentration gradients formed by the three drugs in the chip caused the spatial difference in the MDA-MB-231-RFP cell numbers and migration. The inhibitory effect of combination drugs on cancer cells is more substantial than that of the single drug alone, and this effect of paclitaxel +gemcitabine is more effective than that of paclitaxel+7rh.

Besides, to further illustrate that the CCEC system could evaluate different schemes of combined chemotherapy settings, we chose another anti-cancer drug group, PTX+5-Fu + PP2 [Fig. 4(a)], for testing. Among them, PTX was selected and regarded as the key drug in this drug group. Fluorouracil (5-Fu), like paclitaxel, is also one of the most used anti-cancer drugs in breast cancer.[41] Paclitaxel combined with fluorouracil also has been used clinically.[42] PP2 is an Src kinase inhibitor, which can enhance the expression of E-cadherin (E-cad), activates the function of the E-cad-mediated cell adhesion system, and inhibits the proliferation and migration of cancer cells, PP2 is not currently used in clinical practice.[43,44] After experiments, we found that the concentration gradients formed by paclitaxel, fluorouracil, and PP2 in different regions had spatially differentiated effects on the numbers and migration of MDA-MB-231 cell [shown in Fig. 4(b)]. At the same time, the inhibitory effect of composite drugs on the numbers and migration of MDA-MB-231 cell in the corresponding regions was greater than that of single drugs, which was consistent with the trend observed in the PTX+GEM+7rh group [shown in Figs. 4(c) and 4(d)]. Shapiro–Wilks test and Kolmogorov–Smirnov test were conducted on the cell fluorescence intensity rates under drug groups PTX+5-Fu+PP2 and PTX+GEM+7rh (Fig. S4 in the supplementary material), which were in accordance with the normal distribution. A few of the outliers were derived from experimental errors. By loading two groups of anti-cancer drugs into the chip and analyzing their effects on the numbers and migration of MDA-MB-231 cell, it is shown that our CCEC system is very suitable for high-throughput analysis of cell responses to different drugs. In particular, the 192 collagen microchambers constructed by this chip system can study both the effects of drugs on cell numbers and the effects of drugs on cell migration, which makes the CCEC system unique from other 2D or 3D drug screening systems.

C. Statistical analysis of cell dynamics

In general, the concentration of drugs at a location is related to the distance of drug diffusion. The farther the drug was from the source channel, the lower its concentration. Here, to analyze the effects of individual drugs on cells, as well as the distribution of these in our design, we divided the single drug regions (a_1–c_1, a_2–c_2) and the drug-free regions (d_1, d_2) into four quadrants (Q_1, Q_2, Q_3, Q_4), and characterized the numbers and migration behavior of cell by calculating the fluorescence intensity rate of cells in each quadrant at 120.0h. As shown in the left of Figs. 5(a) and 5(b), for the two groups of anti-cancer drugs PTX+GEM+7rh and PTX+5-FU+PP2, the fluorescence intensity rate of cell numbers and migration in single drug regions gradually increased from Q_1 to Q_4. At the same time, it did not have a noticeable gradient variation in the drug-free regions, and the fluorescence intensity rate in drug-free regions is higher than that in the single-drug regions.

Moreover, in the case of composite drugs, due to the boundary of adjacent drugs represents the region with the most effective drug combination, which has the most effect on cells. Therefore, we selected the four corners (Q_I, Q_{II}, Q_{III}, and Q_{IV}) in the composite drug region (e_1, e_2) under two groups of anti-cancer drugs to further quantify the fluorescence intensity rate of cells and analyze the inhibitory effects between single and composite drugs of two anti-cancer drug groups. The results were showed in Figs. 5(a) and 5(b). For the PTX+GEM+7rh group, the fluorescence intensity rate of Q_I and Q_{II} in Region (e_1) was lower than that of Q_1 in regions (a_1–c_1). Similarly, for the PTX+5-FU+PP2 group, the fluorescence intensity rate of Q_I and Q_{II} in Region (e_2) was also lower than that of Q_1 in regions (a_2–c_2). Meanwhile, the fluorescence intensity rate of partial quadrants (Q_{III} and Q_{IV} for PTX+GEM +7rh and PTX+5-FU+PP2) in composite drugs was higher than that of the corresponding quadrant (Q_1) of the single drug, which may be due to the dilution of the medium in the adjacent channel, leading to its weakened inhibitory effect on cells. These results indicate that the combination of PTX+GEM+7rh and PTX+5-FU+PP2 has a more substantial inhibitory effect on MDA-MB-231 cells than for single drugs. In addition, by comparing the composite drug corners (Q_I, Q_{II}) of the two composite drug regions (e_1, e_2), we found that the fluorescence intensity rates of Q_I in region (e_1) and Q_I, Q_{II} in region (e_2) are significantly lower than that of Q_{II} in region (e_1), indicating that the paclitaxel+gemcitabine, paclitaxel +fluorouracil, and paclitaxel+PP2 have better cell numbers and migration inhibition effect than paclitaxel+7rh. This also indicates that our CCEC system has the potential to evaluate both combination and single drugs simultaneously.

D. Effects of drug gradients on the expression of DDR1 and E-Cad in MDA-MB-231-RFP cells

In biology, combining immunofluorescence and microscopy imaging technologies allows the evaluation of intracellular proteins' expression and studying the influence of external factors on cells.[45] In our study, the effects of drug concentration gradients on cell numbers and migration were assessed by characterizing drug-related proteins. Due to the 7rh and PP2 could inhibit the proliferation and migration of cancer cells by inhibiting the expression of DDR1[46] and enhancing the expression of E-Cad to activate the E-Cad-mediated cells adhesion,[47] respectively. Here, we selected DDR1 and E-cad as the biomarker of PTX+GEM+7rh and PTX +5-Fu+PP2, and labeled them with yellow fluorescence dye and blue fluorescence dye, respectively. Therefore, under the confocal microscope, we were able to obtain the overlay fluorescence image of DDR1 (yellow) and E-cad (blue) in MDA-MB-231-RFP (red) cells in each microchamber region and adjacent matrix region of the biochip [Figs. 6(a) and 6(c)]. As expected, DDR1 is less expressed on the side close to 7rh, while E-CAD is more expressed on the side close to PP2, indicating that the concentration gradients formed by the two drugs in the chip affect the protein expression of the cells.

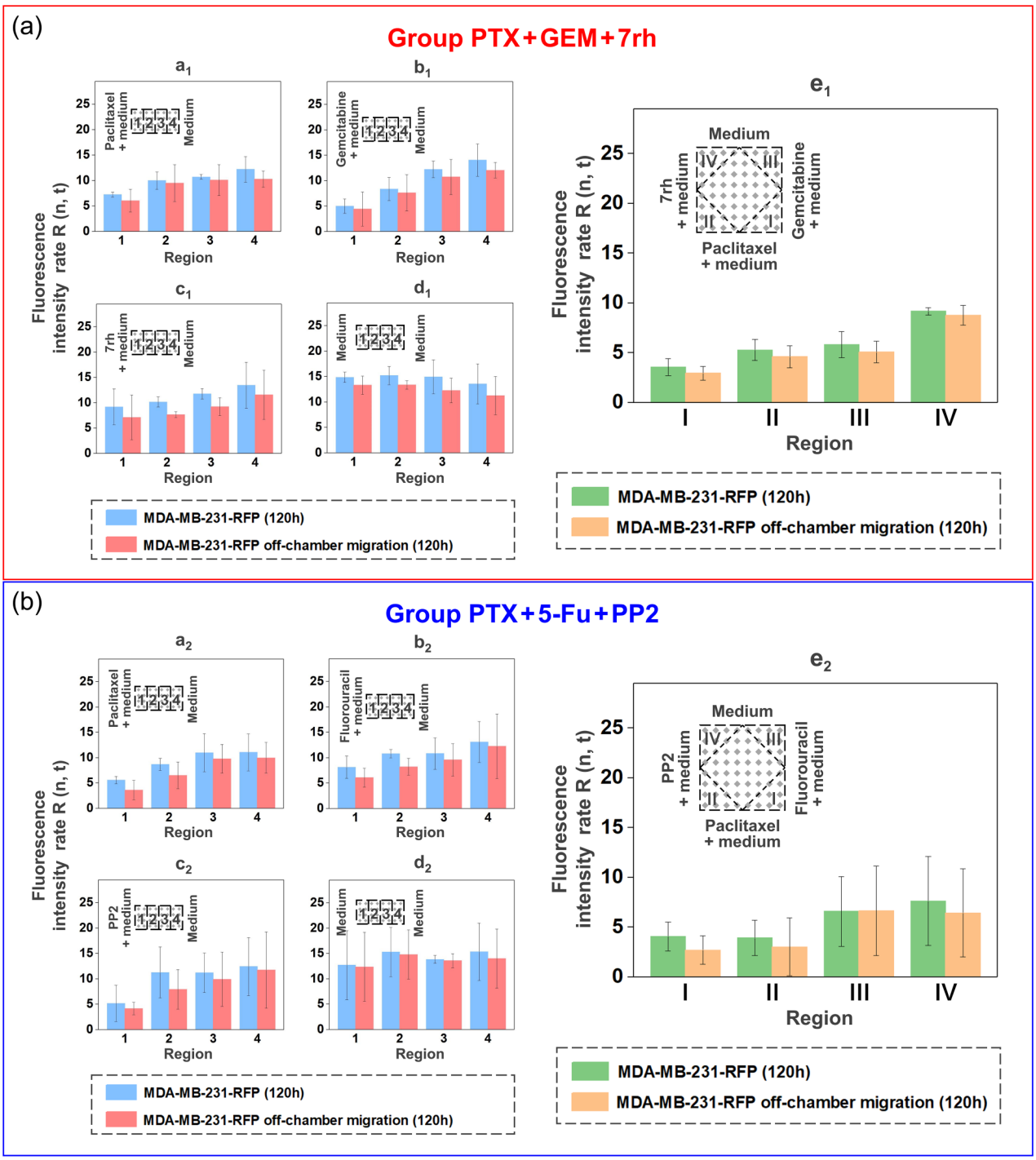

FIG. 5. The division and statistical analysis of each region in the chip according to the distribution of drug concentration gradients. (a) In the PTX+GEM+7rh group, the (a_1)–(d_1) region is divided into four quadrants (Q_1–Q_4) along with the drug diffusion or medium penetration direction, respectively. MDA-MB-231-RFP cell numbers in each quadrant (blue) and the migration out of the microchamber (red) are counted. The four quadrants (Q_I–Q_{IV}) in the (e_1) region have higher concentrations of composite drugs. The numbers (green) and migration off the microchambers (orange) of MDA-MB-231-RFP cell in each quadrant are counted. (b) The PTX+5-Fu+PP2 group is analyzed using the same statistical method.

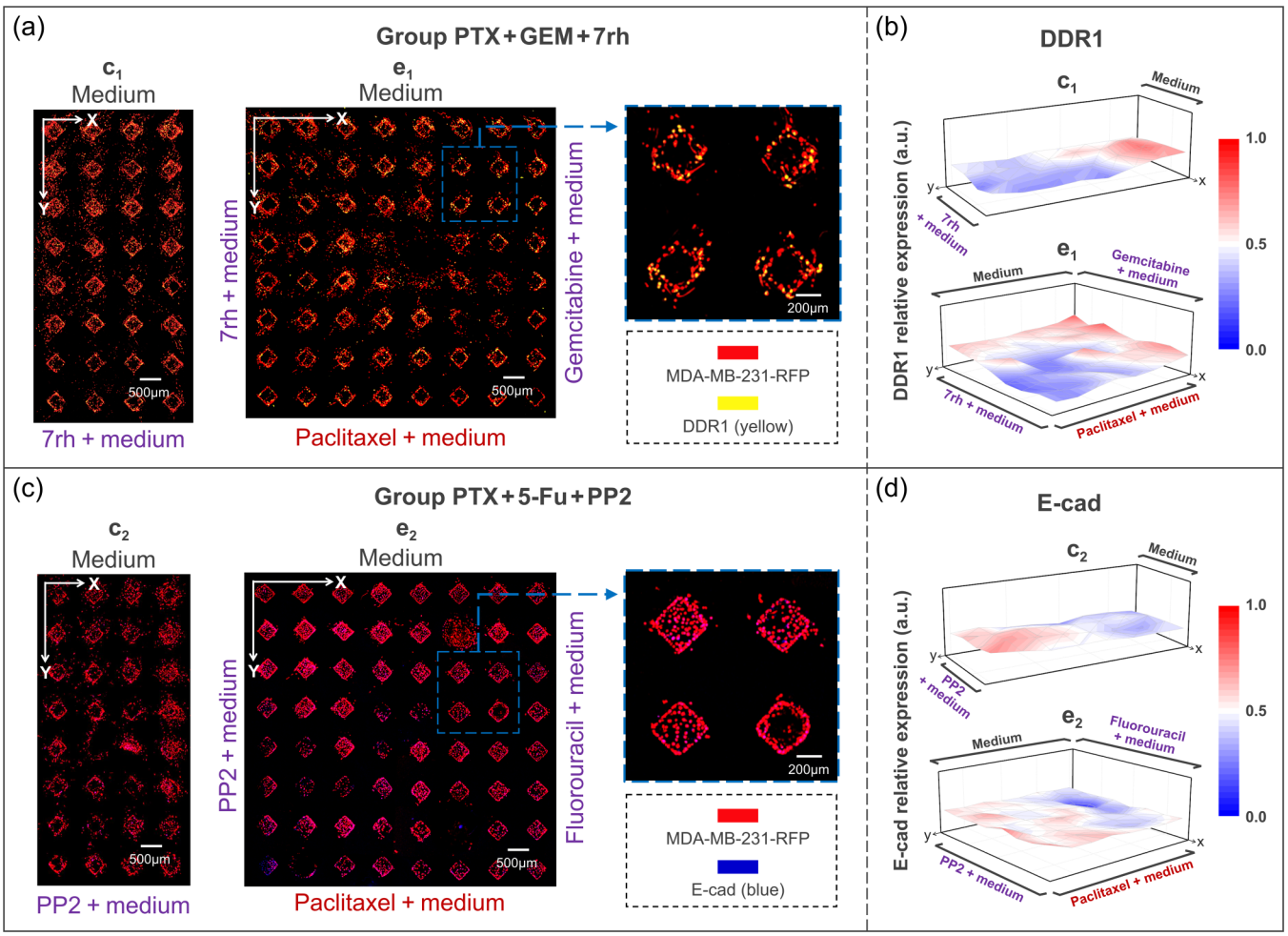

FIG. 6. Immunofluorescence analysis of cellular proteins. (a) Merged fluorescence images of MDA-MB-231-RFP cells (red) and DDR1 protein (yellow) in the (c_1) and (e_1) regions of the PTX+GEM+7rh group at 120.0 h. (b) The spatial distribution of the relative expression of DDR1 protein in the (c_1) and (e_1) regions. (c) Composite fluorescence images of MDA-MB-231-RFP cells (red) and E-cad protein (blue) in the (c_2) and (e_2) regions of the PTX+5-Fu+PP2 group at 120.0 h. (d) The spatial distribution map of the relative expression of E-cad protein in the (c_2) and (e_2) regions. The scale bar from blue to red indicates the relative expression of protein from low to high.

Moreover, to analyze the distribution of relative expression levels of DDR1 protein and E-cad protein further quantitatively, we divided (c_1) and (c_2) regions into 32 sub-regions and divided the (e_1) and (e_2) regions into 64 sub-regions, respectively. Then, the relative protein expression was quantified by MATLAB software to calculate the fluorescence intensity of each sub-region. As shown in Fig. 6(b), the relative expression of DDR1 in the (c_1) and (e_1) region is lower on the 7rh side (about 0.30), while it is higher on the medium or gemcitabine side (about 0.7), which suggest that 7rh can inhibit the numbers and migration of cancer cell by inhibiting the expression of DDR1. Similarly, for the PTX+5-Fu+PP2 group [Fig. 6(d)], the relative expression of E-cad on the PP2 side is higher in both (c_2) and (e_2) regions (about 0.7), while it is lower on the medium or fluorouracil side (about 0.35), suggesting that PP2 can enhance the expression of E-cad and inhibit the numbers and migration of cancer cell. Besides, comparing the relative expression of DDR1 and E-Cad proteins under the single drugs with composite drug conditions, the protein expression of DDR1 in the single drug region was slightly lower than that in the corresponding region of composite drugs. In contrast, the expression of E-Cad exhibited the opposite situation. These results of protein expression in MDA-MB-231-RFP cells under the drug concentration gradients were consistent with the above statistical analysis results, indicating that the effects of drugs indirectly reflect the inhibition of 7rh and PP2 drugs on cell numbers and migration on cell proteins. Therefore, the CCEC system can assess high-throughput drug-related proteins, evaluate the mechanism of drugs, and provide an efficient platform for preclinical drug screening.

IV. CONCLUSION

The CCEC system contains the closed microchamber and stable composite/single drug concentration gradient constructed by the collagen microenvironment. Under the drug concentration gradient, each microchamber and the cells in the microchamber are in a unique local biochemical microenvironment. Through microscopy imaging, the system enables high-throughput comparative analysis of cellular dynamic behavior under the composite and single drug concentration gradient at the same chip to effectively evaluate the effectiveness of combination chemotherapy regimens. Coupled with immunofluorescence technology, the system can characterize drug-related proteins and evaluate cell response to drugs by analyzing cell behavior and protein expression. In summary, the CCEC system can be a novel drug screening platform that works efficiently. It also provided a preliminary evaluation of the effects of combination chemotherapy or one of the drugs on cells in a biomimetic microenvironment.

In addition, by changing the internal structure of the bionic microenvironment and the types of cells in the microchamber, the chip can be applied to the biological research of various tumors and the evaluation of combined chemotherapy regimens. In particular, the implantation of patient-derived tumor cells or tumor organoids into the microchamber can explore the pathological features of tumors in the patient's body and further evaluate the efficacy of combined chemotherapy regimens to provide optimal treatment. Therefore, the CCEC system may provide a new platform for personalized therapy.

SUPPLEMENTARY MATERIAL

See the supplementary material (Fig. S1) for the SEM image of 5.0 mg/ml collagen. Figures S2 and S3 show the quantification process of cell numbers and migration, respectively. Figure S4 shows the statistical test analysis.

ACKNOWLEDGMENTS

We gratefully acknowledge support by the National Natural Science Foundation of China (NNSFC) (Nos. 11974066, 12174041, and 12104134) and the Fundamental and Advanced Research Program of Chongqing (No. cstc2019jcyj-msxmX0477), Fundamental Research Funds for the Central Universities (No. 2022CDJJCLK001), and a start-up fund (No. OJQD2022005). Besides, we would like to thank Miss Qin Deng at the Analytical and Testing Center of Chongqing University for her assistance with immunofluorescence imaging and analysis.

AUTHOR DECLARATIONS

Conflict of Interest

The authors have no conflicts to disclose.

Author Contributions

J.Y. and G.L. contributed equally to this work.

Jingru Yao: Conceptualization (equal); Data curation (lead); Formal analysis (lead); Methodology (lead); Validation (equal); Visualization (equal); Writing – original draft (lead); Writing – review & editing (equal). **Guoqiang Li:** Conceptualization (equal); Formal analysis (equal); Writing – original draft (equal); Writing – review & editing (equal). **Lianjie Zhou:** Data curation (equal); Methodology (equal). **Shuyan Xu:** Methodology (equal); Writing – original draft (equal); Writing – review & editing (equal). **Kena Song:** Writing – original draft (supporting); Writing – review & editing (supporting). **Hongfei Zhang:** Formal analysis (equal); Visualization (equal). **Xianquan Zhang:** Formal analysis (equal); Visualization (equal). **Jianwei Shuai:** Writing – original draft (equal); Writing – review & editing (equal). **Fangfu Ye:** Writing – original draft (equal); Writing – review & editing (equal). **Ming Li:** Writing – original draft (equal); Writing – review & editing (equal). **Guo Chen:** Methodology (equal); Visualization (equal). **He Liu:** Writing – original draft (equal); Writing – review & editing (equal). **Peter Shaw:** Formal analysis (supporting); Writing – original draft (equal); Writing – review & editing (equal). **Liyu Liu:** Conceptualization (equal); Data curation (equal); Writing – review & editing (equal).

DATA AVAILABILITY

The data that support the findings of this study are available from the corresponding authors upon reasonable request.

REFERENCES

[1]D. Liu, X. Liu, Y. Zhang, Q. Wang, and J. Lu, Bioengineered **7**(5), 321–326 (2016).
[2]A. J. Redig and S. S. McAllister, J. Intern. Med. **274**(2), 113–126 (2013).
[3]X. Yue, T. D. Nguyen, V. Zellmer, S. Zhang, and P. Zorlutuna, Biomaterials **170**, 37–48 (2018).
[4]S. Talukdar and S. C. Kundu, Adv. Funct. Mater. **22**(22), 4778–4788 (2012).
[5]A. L. Radtke and M. M. Herbst-Kralovetz, J. Vis. Exp. **62**, e3868 (2012).
[6]J. S. Harunaga and K. M. Yamada, Matrix Biol. **30**(7–8), 363–368 (2011).
[7]H. Tian, J. Pang, K. Qin, W. Yuan, J. Kong, H. Ma, J. He, X. Yang, Y. Luo, Y. Lu, B. Lin, and T. Liu, Biotechnol. J. **15**(2), 1900107 (2020).
[8]X. J. Li, A. V. Valadez, P. Zuo, and Z. Nie, Bioanalysis **4**(12), 1509–1525 (2012).
[9]O. E. Atat, Z. Farzaneh, M. Pourhamzeh, F. Taki, R. Abi-Habib, M. Vosough, and M. El-Sibai, Hum. Cell **35**(1), 23–36 (2022).
[10]K. M. Yamada and E. Cukierman, Cell **130**(4), 601–610 (2007).
[11]X. Zhang, M. Karim, M. M. Hasan, J. Hooper, R. Wahab, S. Roy, and T. A. Al-Hilal, Cancers **14**(3), 648 (2022).
[12]E. Lee, H. G. Song, and C. S. Chen, Curr. Opin. Chem. Eng. **11**, 20–27 (2016).
[13]R. Kalot, R. Mhanna, and R. Talhouk, Pharmacol. Ther. **237**, 108156 (2022).
[14]N. Dhiman, P. Kingshott, H. Sumer, C. S. Sharma, and S. N. Rath, Biosens. Bioelectron. **137**, 236–254 (2019).
[15]H. Wang, G. Tan, L. Dong, L. Cheng, K. Li, Z. Wang, and H. Luo, Plos One **7**(4), e34210 (2012).
[16]K. M. Ibiyeye, N. Nordin, M. Ajat, and A. B. Z. Zuki, Front. Oncol. **9**, 599 (2019).
[17]S. S. Qi, J. H. Sun, H. H. Yu, and S. Q. Yu, Drug Deliv. **24**(1), 1909–1926 (2017).
[18]D. L. Jardim, D. D. M. Gagliato, M. Nikanjam, D. A. Barkauskas, and R. Kurzrock, Oncolmmunology **9**(1), e1710052 (2019).
[19]C. M. Bachelard, E. Coquan, P. Rusquec, X. Paoletti, and C. L. Tourneau, EClinicalMedicine **40**, 101130 (2021).
[20]M. K. Yan, N. R. Adler, N. Heriot, C. Shang, J. R. Zalcberg, S. Evans, R. Wolfe, and V. J. Mar, Asia-Pac. J. Clin. Oncol. **18**(4), 344–352 (2022).
[21]D. B. Fogel, Contemp. Clin. Trials Commun. **11**, 156–164 (2018).

[22]T. Baltazar, N. S. Kajave, M. Rodriguez, S. Chakraborty, B. Jiang, A. Skardal, V. Kishore, J. S. Pober, and M. Z. Albanna, J. Biomed. Mater. Res. B Appl. Biomater. **110**(10), 2323–2337 (2022).
[23]O. De Wever, A. Hendrix, A. De Boeck, W. Westbroek, G. Braems, S. Emami, M. Sabbah, C. Gespach, and M. Bracke, Int. J. Dev. Biol. **54**(5), 887–896 (2010).
[24]W. Sun, C. T. Lim, and N. A. Kurniawan, J. R. Soc. Interface **11**(99), 20140638 (2014).
[25]J. Plou, Y. Juste-Lanas, V. Olivares, C. delAmo, C. Borau, and J. M. Garcia-Aznar, Sci. Rep. **8**(1), 12723 (2018).
[26]J. E. Kim, D. S. Reynolds, M. H. Zaman, and M. Mak, Integr. Biol. **10**(4), 232–241 (2018).
[27]J. Yao, G. Li, Y. Jiao, Y. Zheng, Y. Liu, G. Wang, L. Zhou, H. Zhang, X. Zhang, J. Shuai, Q. Fan, F. Ye, S. Lou, G. Chen, K. Song, Y. Liao, and L. Liu, Lab Chip **21**(15), 3004–3018 (2021).
[28]M. R. Carvalho, D. Barata, L. M. Teixeira, S. Giselbrecht, R. L. Reis, J. M. Oliveira, R. Truckenmüller, and P. Habibovic, Sci. Adv. **5**(5), eaaw1317 (2019).
[29]Y. Pei, X. Wang, W. Huang, P. Liu, and L. Zhang, Cellulose **20**(4), 1897–1909 (2013).
[30]Y. Jiao and S. Torquato, Phys. Biol. **9**(3), 036009 (2012).
[31]T. M. Abu Samaan, M. Samec, A. Liskova, P. Kubatka, and D. Busselberg, Biomolecules **9**(12), 789 (2019).
[32]S. Murray, E. Briasoulis, H. Linardou, D. Bafaloukos, and C. Papadimitriou, Cancer Treat. Rev. **38**(7), 890–903 (2012).
[33]C. Delfino, G. Caccia, L. R. Gonzales, E. Mickiewicz, J. Rodger, L. Balbiani, D. F. Morales, A. Z. Comba, and C. Brosio, Oncology **66**(1), 18–23 (2004).
[34]B. Wirk and E. Perez, Semin. Oncol. **33**(1), S6–S14 (2006).
[35]M. Gao, L. Duan, J. Luo, L. Zhang, X. Lu, Y. Zhang, Z. Zhang, Z. Tu, Y. Xu, X. Ren, and K. Ding, J. Med. Chem. **56**(8), 3281–3295 (2013).
[36]Q. P. Lu, W. D. Chen, J. R. Peng, Y. D. Xu, Q. Cai, G. K. Feng, K. Ding, X. F. Zhu, and Z. Guan, Oncol. Lett. **12**(5), 3598–3608 (2016).
[37]B. Xiao, L. Ma, and D. Merlin, Expert Opin. Drug Deliv. **14**(1), 65–73 (2017).
[38]F. Cappuzzo, F. Mazzoni, A. Gennari, S. Donati, B. Salvadori, C. Orlandini, G. L. Cetto, A. Molino, E. Galligioni, M. Mansutti, S. Tumolo, A. Lucentini, F. Valduga, S. Bartolini, L. Crino, and P. F. Conte, Br. J. Cancer **90**(1), 31–35 (2004).
[39]K. Y. Aguilera, H. Huang, W. Du, M. M. Hagopian, Z. Wang, S. Hinz, T. H. Hwang, H. Wang, J. B. Fleming, D. H. Castrillon, X. Ren, K. Ding, and R. A. Brekken, Mol. Cancer Ther. **16**(11), 2473–2485 (2017).
[40]A. Krtolica, C. O. D. Solorzano, S. Lockett, and J. Campisi, Cytometry **49**(2), 73–82 (2002).
[41]W. Zhang, M. Feng, G. Zheng, Y. Chen, X. Wang, B. Pen, J. Yin, Y. Yu, and Z. He, Biochem. Biophys. Res. Commun. **417**(2), 679–685 (2012).
[42]N. Yamamoto, P. Jiang, M. Yang, M. Xu, K. Yamauchi, H. Tsuchiya, K. Tomita, G. M. Wahl, A. R. Moossa, and R. M. Hoffman, Cancer Res. **64**(12), 4251–4256 (2004).
[43]M. P. Sanchez-Bailon, A. Calcabrini, D. Gomez-Dominguez, B. Morte, E. Martin-Forero, G. Gomez-Lopez, A. Molinari, K. U. Wagner, and J. Martin-Perez, Cell. Signal. **24**(6), 1276–1286 (2012).
[44]J. S. Nam, Y. Ino, M. Sakamoto, and S. Hirohashi, Clin. Cancer Res. **8**(7), 2430–2436 (2002).
[45]Y. H. Chan, G. J. Chang, Y. J. Lai, W. J. Chen, S. H. Chang, L. M. Hung, C. T. Kuo, and Y. H. Yeh, Cardiovasc. Diabetol. **18**(1), 125 (2019).
[46]L. Castro-Sanchez, A. Soto-Guzman, M. Guaderrama-Diaz, P. Cortes-Reynosa, and E. P. Salazar, Clin. Exp. Metastasis **28**(5), 463–477 (2011).
[47]E. G. Graham, E. M. Wailes, and N. H. Levi-Polyachenko, J. Biomed. Nanotechnol. **12**(2), 308–319 (2016).